Korean J. Chem. Eng., **27**(2), 511-517 (2010)
DOI: 10.1007/s11814-010-0085-y

Evaluation of the buffing volume in last third flocculation basin using CFD

Youngman Cho*,†, Soojeon Yoo*, Youngdo Hwang*, Jaesoon Roh*, Pyeongjong Yoo*, and Changwon Kim**

*Water Quality Research of Busan Water Authority, Kimhae, Gyeongnam 621-813, Korea
**Department of Environment Engineering, Pusan National University, Busan 609-735, Korea
(*Received 1 April 2009 • accepted 3 September 2009*)

Abstract−In Korea, the party walls of the flocculation basin consist generally of four parts, as three party walls and the outlet wall. The space between the third party wall and the outlet wall is therefore not the full extent of the flocculation basin and sedimentation basin. This space is theoretically totally unfounded. In order to practically apply the third party wall as an outlet wall, the volume capacity of the last third flocculation process needs to be determined on the ground that the perforated baffle (opening ratio 6%) is not ideal for the rectification effect. The buffer zone, according to the G value, is required in the last third flocculation process for a uniform flow at the outlet. Therefore, the objective of this study was to determine the size of the buffer zone in the last third flocculation process using CFD. Conclusions are made as follows: The difference of outflow rate percentage between the upper, middle and bottom part sections reduces according to the expansion of the third basin volume from 4.2 to 7.7 at each G value. We can suggest that the effluent percentage at the three sections is less affected by the G value than by the volume increase. For G values ranging from 11 to 16(1/s), the buffer zone needs to range from 10% to 20% compared with the last third volume by the velocity of standard deviation of 5 at the outlet. Also, when the velocity of standard deviation at the outlet is 2.5 or less, the buffer zone needs to range from 45% to 55%.

Key words: Flocculation, Buffer Zone, Computational Fluid Dynamics (CFD)

INTRODUCTION

Flocculation is dependent on the duration and amount of gentle agitation applied to the water. In flocculation basins, the fine microfloc begins to agglomerate into larger, dense, rapid-settling floc particles [1]. In Korea, the types of devices usually used to furnish the agitation are generally mechanical agitators, such as paddles.

Flocculation basins are frequently designed to provide for tapered flocculation in which the flow is highly subjected to decreasing velocity gradient (G) values as it passes through the flocculation basin. This produces a rapid buildup of small, dense floc, which subsequently aggregates at lower G values into larger floc particles. Tapered flocculation is usually accomplished by providing a high G value during the first third flocculation interval, a lower G value during the next third, and much lower G values during the last third. Although many basins are designed that have tapered flocculation, optimum flocculation usually necessitates its use [2]. Typical arrangements for flocculators are paddle wheels on horizontal shafts and at least three consecutive compartments are required to minimize short circuiting. The partitions wall is usually concrete perforated baffle type.

In Korea, the party walls of the flocculation basin generally consist of the four parts as three party walls and the final outlet wall. The space (Fig. 1 ↘) between the third party wall and the final outlet wall is therefore not the full extent of the flocculation basin and sedimentation basin. The upper area of this space is covered with concrete and used as a passageway. This space is theoretically totally unfounded. Because there is no flocculator at this space, the formed floc settle. Therefore, with time, the floc accumulate on the bottom of the flocculation basin. Accumulated floc are only removed by cleaning the flocculation basin once a year. In addition, accumulated floc fill up the hole of the outlet wall, causing an upward flow at the outlet perforated baffle. This flow affects the efficiency of sedimentation. The efficiency of sedimentation is affected by the inlet energy, turbidity, the water temperature, and weather conditions. The inlet energy is the most important factor among the influencing factors [3]. Therefore, this space should be removed in order to prevent the settlement of floc at this volume. However, in order to practically apply the third party wall as an outlet wall, the volume capacity of the last third flocculation process needs to be determined. This is because the perforated baffle is not ideal for the rectification effect. So if the buffer zone is in the last third flocculation basin, the effluent flow of the flocculation basin is more uniform. Therefore, we evaluated the size of the buffer zone in the last third flocculation basin according to the G value.

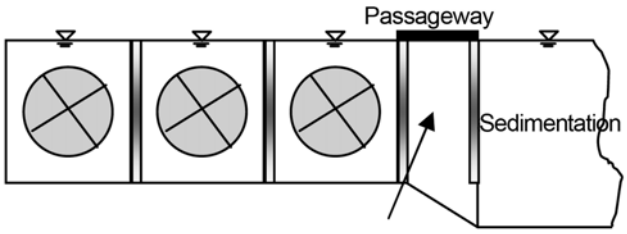

Fig. 1. A cross section of flocculation basin.

In this study, we conducted a computational fluid dynamics (CFD) simulation. CFD is a valuable tool for quickly extracting accurate

†To whom correspondence should be addressed.
E-mail: chol221@korea.kr

information about turbulent flow and mixing in industrially relevant devices, the complex geometries of which would have, only a few years ago, prevented modeling [4]. Recently, CFD has been accepted as a useful tool for the modeling of water treatment systems [5]. Therefore, the objective of this study is to determine the need and the size of the buffer zone in the last third flocculation process using CFD.

MATERIALS AND METHODS

The flocculation basin of this study is located in Busan, Korea. The size of the flocculation basin is B12 m×L14.7 m×H4.0 m. HRT, flocculator is 50 min and paddle wheels on horizontal shafts (3 step), respectively. Basic volume of one step in the flocculation basin is B12 m×L4.2 m×H4 m and this space (Fig. 1↘) is B12 m×L2.1 m×H4 m. The flocculator's spin is in a clock-wise direction. The partition wall is perforated baffle and the ratio of the orifice (Φ=10 mm) area to the cross-sectional area of the baffle is 6%. The limit of simulation in this study is from the first step to the third step of the flocculation basin. So we removed the space (Fig. 1↘) in simulation. Instead, we increased the length of last third flocculation basin from 4.2 m to 7.7 m by 0.5 m for decision of the buffer zone. G values in the volume of the third basin are 7(1/s), 11(1/s), 16(1/s), 20(1/s), and 26(1/s), respectively. Table 2 indicates the rotational speed according to G value and length in the third step. The equation for the velocity gradient is

$$G=(P/uV)^{0.5}$$

$$P=C_D A\rho v^3/2$$

where

P=power imparted to the water (N-m/s)
V=basin volume (m^3)
u=absolute viscosity of the water
C_D=coefficient of drag, (1.50- at the length-width ratio 20)
A=paddle blade area at right angle to the direction of movement (m^2)
ρ=density of the water
v=velocity of the paddle blade relative to the water (rps)

Table 1. The operation parameter of flocculation basin

Items	Operation parameter
Basin size	B12 m×L14.4 m×H4.0 m
HRT	50 min,
Flocculator	Paddle wheels, on horizontal shafts (3 step)
G value (s^{-1})	1 step (50) 2 step (26) 3 step (7, 11, 16, 20, 26)
Spin	1, 2 step clockwise, 3 step counterclock-wise

Table 2. Rotational speed (rpm) according to the G value and length in third step

G value (s^{-1})					
Length (m)	7	11	16	20	26
4.2	0.59	0.79	1.02	1.18	1.41
4.7	0.61	0.82	1.06	1.23	1.46
5.2	0.63	0.85	1.09	1.27	1.51
5.7	0.65	0.88	1.13	1.31	1.56
6.2	0.67	0.90	1.16	1.35	1.60
6.7	0.69	0.93	1.19	1.38	1.65
7.2	0.70	0.95	1.22	1.41	1.69
7.7	0.72	0.97	1.25	1.45	1.73

In the late 1970s, the development and availability of new high speed computers and new computational techniques made it possible to numerically solve the basic Navier-Stokes equation [6]. In this present study, model development and simulation were based on commercial CFD software, Fluent 6.3, and meshing software, Gambit 2.4 (Fluent Inc., NH, USA). Fluent 6.3, which is a finite-volume code, was used in hydrodynamics and mass transfer computations, while Gambit 2.4 provided complete mesh flexibility in solving flow problems with both structured and unstructured meshes. All functions required to compute a solution and display the results in the Fluent software are accessible either through an interactive interface or by constructing user-defined-functions (UDS) [7,8].

In the CFD simulation of water treatment flow, the K-Epsilon model is generally used. This model is used in the commercial CFD code, and is comprised of K, of the granular temperature equation, and epsilon, of the conservation law. An immediate benefit of the realizable K-Epsilon model is that it more accurately predicts the spreading rate of both planar and round jets. It is also likely to provide superior performance for flows involving rotation, boundary layers under strong adverse pressure gradients, separation, and recirculation [8-10]. The governing equations are based on the equation of continuity and the equation of momentum conservation, which is the Navier-Stokes Equation. The assumptions used for solving the above equations included: (1) steady state operation, (2) turbulent flow regime (Realizable k-ε), and (3) non-slip boundary conditions at wall surfaces. The boundary conditions of inlet and outlet were velocity inlet and pressure outlet, respectively. The flocculator spin was the moving reference frame at the motion type in the boundary condition. The flocculator spin was multiple rotating reference frames (MRF) at the motion type in the boundary condition. Hence, MRF approach is considered as steady-state approximation and the sliding mesh model approach, on the other hand, is inherently unsteady due to the motion of the mesh with time. The MRF approach was found to be sufficient to develop an understanding of the magnitude of velocity gradients to which a floc may be subjected within a vessel [11]. The dimension of simulation was 3D. The count of volume mesh is 1,245,392. We used the species transport method in the Fluent software for the evaluation of hydrodynamic behavior. This method can be used to model the mixing and transport of chemical species by solving conservation equations that describe convection, diffusion, and reaction sources for each component species. FLUENT predicts the local mass fraction of each species, Yi, through the solution of a convection-diffusion equation for the ith species. The convection, diffusion, and reaction sources can be bypassed in the equation. The species equation is the same as Eq. (1). Here, Yi is the local mass fraction and Ji is the diffusion flux of species I [10].

$$\frac{\delta}{\delta t}(\rho \mathrm{Yi}) + \nabla(\rho \mathrm{v} - \mathrm{Yi}) = -\nabla(\mathrm{Ji}^{\rightarrow}) \quad (1)$$

The species transport method in the Fluent is similar to the meth-

od used in the trace test. After finishing simulation of the flow and turbulence in the steady state, under the results, the species transport is simulated in the unsteady state. We selected water as the chemical species. First, the species (water) was poured into the inlet port for five seconds. Second, the concentration of output was collected at the outlet every one second.

The reliability and accuracy of CFD simulation was investigated by comparison with experimental data. We used sodium fluoride for the tracer test. After the sodium fluoride was dissolved in water, it was rapidly poured at the inlet of the flocculation basin. We sampled the output water at 5-minute intervals at the outlet of the flocculation basin and measured the fluoride ion concentration by ion chromatography. The sampling port was fifty centimeters in front of the third wall and one meter under the water surface and from the side wall.

RESULTS AND DISCUSSION

1. Comparison of CFD Simulation and Experimental Results

The reliability and accuracy of CFD simulation was investigated by comparison with experimental data (Fig. 2). The recovery ratio of fluoride ion was 96% in the tracer test. The t in Fig. 2 shows effluent time of species (CFD simulation) or trace (experimentation) and to is HRT (50 minute). The C and Co are effluent concentration and total concentration (total amount of the influent species or trace/volume of flocculation basin), respectively. The result data showed an almost similar trend to both the CFD simulation and the experimental data. The start and maximum points are the same. However, for the CFD simulation date, the concentration was reduced more rapidly than that of the experimental date after the maximum point was reached. This result proved application of the CFD simulation data.

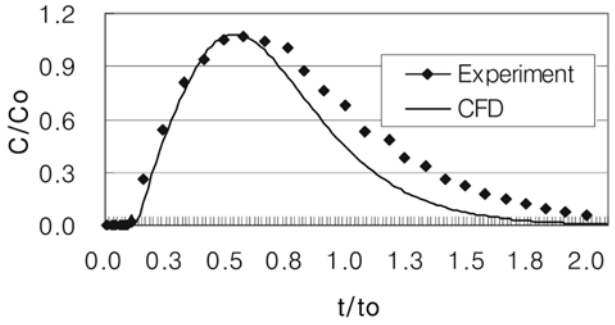

Fig. 2. Comparison of CFD simulation and experimental data.

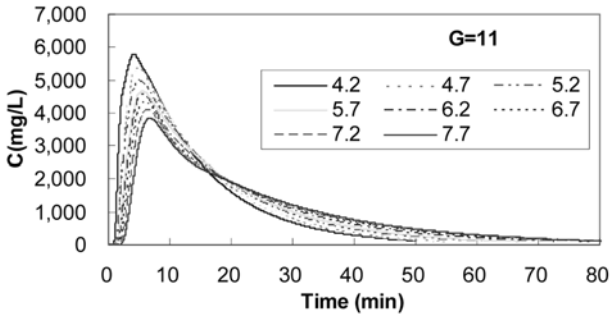

Fig. 3. The effluent concentration of species at G value 11(1/s).

2. Flow Characteristics According to the Volume of the Third Basin

Fig. 3 indicates the effluent concentration of 'species' at G value 11(1/s) when increasing the length of the third basin from 4.2 m to 7.7 m. As the volume of the third basin continues to increase, the concentration at the peak point is reduced, and the effluent time is delayed. This is due to the following reasons. Although the volume of the third basin increases, the total amount of species remains the same. The expansion of the third basin causes the augmentation of the dilution rate, and thus the initial concentration (Co) of the third basin is lower than that of the original volume.

The delay of effluent time is also the result of the simulation of the third basin, because the hydraulic retention time is extended when the third basin is larger. Thus, if the x axis and the y axis of these graphs are shown as T/To and C/Co (Fig. 2), T/To, C/Co at the peak point of each case will be equal. In addition, the results of species simulation at G values of 7(1/s), 16(1/s), 20(1/s), and 26(1/s) when varying the volume of the third basin are similar to those of the simulation at a G value of 11(1/s).

Fig. 4 is the result of evaluation of the flow characteristics. Firstly, Fig. 4(a) provides the Morrill index, indicating the standard of mixing of flow. The large value of the Morrill index indicates well mixed flow, and 1 indicates plug flow. Fig. 4(a) provides that an increased G value results in the increment of the Morrill index. In the cases of G value 7(1/s), G value 11(1/s), and G value 16(1/s), the value of the Morrill index ranges from 7 to 9, and in other cases of G value 20(1/s) and G value 26(1/s), the value of the Morrill index is about 10. Thus, we can deduce that the augmentation of the G value causes a stronger mixing of flow. In the case of an equal G value, when the volume of the third basin increases, the value of the Morrill index shows a tendency to decrease. This is because the ratio of the region that can be mixed at an equal G value is reduced relatively according to the expansion of the third basin. Moreover, when comparing the effect of the G value and the increase of volume in the Morrill index, the augmentation of the G value results in the increment of the Morrill index. However, while the volume of the third basin increases, the value of the Morrill index rarely varies. From the fact that, we can deduce that the Morrill index is influenced more by the G value rather than by the volume of the basin.

Secondly, Fig. 4(b) provides the modal index indicating the valuation basis of a plug flow, and the value of 1 implies that the flow is a complete plug flow. Fig. 4(b) demonstrates that the increased G value causes the tendency of the modal index to converge to zero, which means that the mixing standard at the basin augments. Although we cannot find evidence that a definite variation of patterns exists, such as a regular increment or decrement according to the expansion of the third basin, there is a slight reduction in the variation of the modal index which is variable by the augmentation of volume. Furthermore, while the variation of the modal index by the G value is high which ranges from 0.18 to 0.38, the range of variation by the expansion of volume is low; approximately 0.05. From these results, it can be considered that, similar to the Morrill index, the modal index is highly influenced by the G value than the volume of the third basin.

Fig. 4(c) illustrates the Short Circuiting Index, in which a large

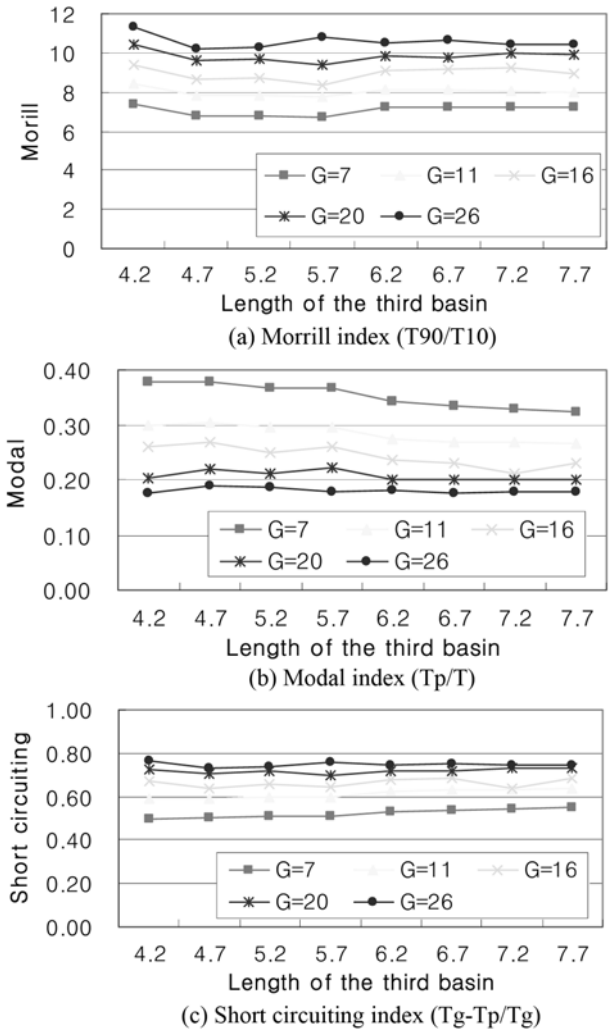

Fig. 4. Morrill, Modal, and Short circuiting indices according to the length of the third basin.

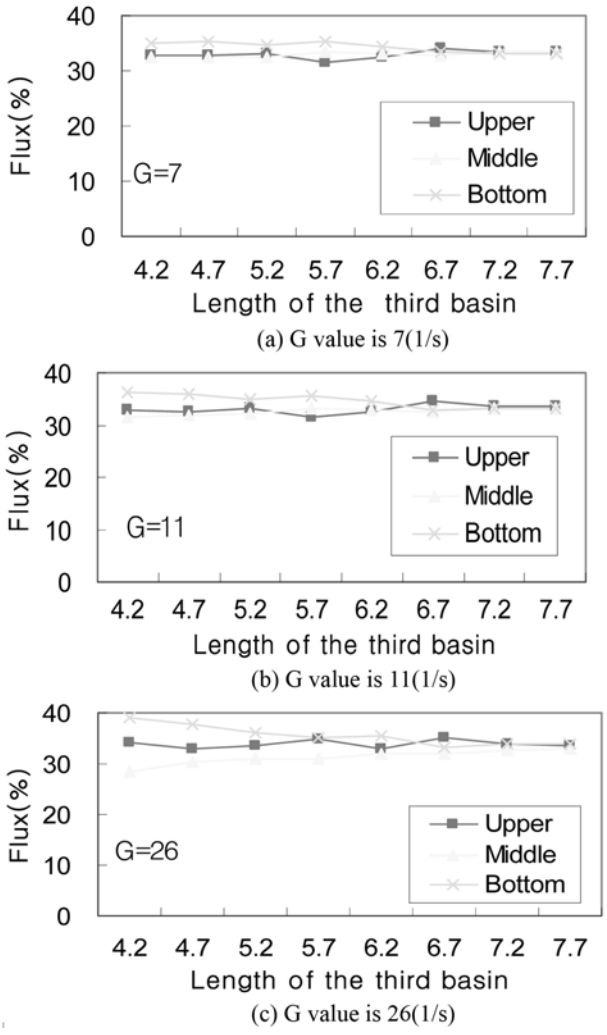

Fig. 5. The effluent Flux at the upper, middle, bottom to the length of the third basin.

value implying a generation of significant amount of short circuiting flow. An obvious increment of the short circuiting index is observed. In contrast, the value of the short circuiting index, in line with the expansion of volume, has an escalating pattern only in the cases of G value 7(1/s) and G value 11(1/s), while cases of G value 20(1/s) and G value 26(1/s), clear variations rarely appeared. These results can be explained as follows. In the case of a low G value, the generation of short circuiting flow increases when the dead space is expanded relatively according to the increment of volume. However, in the case of a high G value, the effect of volume rarely happens due to an extremely strong mixing power. In other words, the augmentation of the G value results in an increment of the short circuiting index unrelated to the volume of the third basin, and the short circuiting flow is augmented according to the expansion of the third basin within a low G value. The variation of the short circuiting index by the G value ranges from 0.5 to 0.76, and the range of this variation by the expansion of volume is about 0.05. In summary, by analyzing the results of simulations for evaluating the indexes, we can deduce that the mixing level and the generation of the short circuiting flow are augmented with the increment of the G value and the expansion of the third basin, and that the flow in the flocculation process is therefore deteriorated. Therefore, we are able to make a potential conclusion that the buffer zone for the third basin of the flocculation process should be minimized in order to produce a uniform flow at the outlet wall.

For the evaluation of the effluent pattern, we divided the perforated baffle into three sections as the upper middle and the bottom part. Fig. 5 presents the effluent flux percentage of the outlet as a result of applying the variation of volume of the third basin at each G value.

Firstly, by analyzing Fig. 5, we can observe that the difference of effluent flux percentages of the three sections is reduced according to the expansion of the third basin volume from 4.2 to 7.7 at each G value. In the case where the length of the third basin is 7.7, the effluent flux percentages of the three sections are mostly equal, at about 33%. In contrast, the difference of the effluent flux percentages of the three sections is over 5% when the volume is close to 4.2.

Similar results can also be presented in Fig. 6. Fig. 6 indicates the standard deviation of the effluent flux percentage of the three

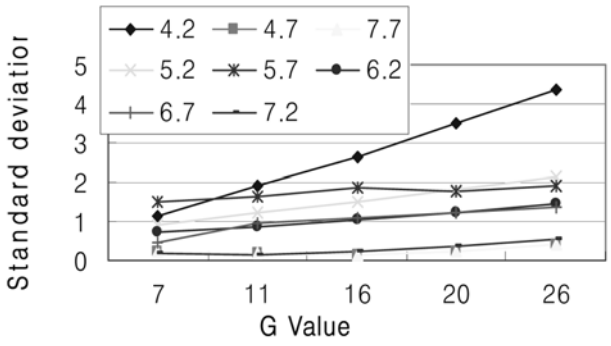

Fig. 6. Standard deviation of the flux according according to the G value.

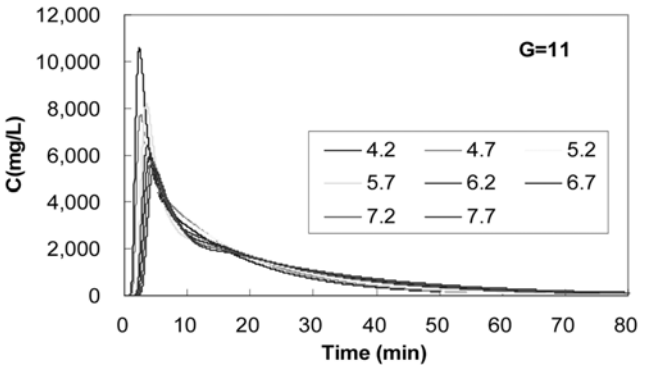

Fig. 8. Flux at upper, middle, bottom at G value 11(1/s) with counterclock-wise.

sections according to the length of the third basin at all G values (7(1/s), 11(1/s), 16(1/s), 20(1/s), and 26(1/s)). The calculation of the standard deviation is described by the following formula:

$$\sigma=\sqrt{\frac{\sum_{k=1}^{n}(x_k-m)^2}{n}}=\sqrt{\frac{\sum_{k=1}^{n}x_k^2}{n}-m^2}$$

Where x denotes the sample and m and n denotes the mean and number of the sample, respectively. In the case where the length of the third basin is 4.2, the variation of effluent flux at the three sections is considerable, yet the standard deviation is not large, at 7.7 of the length. Thus, we can suggest that the effluent flux at the three sections is less affected by the G value than it is by the volume increase.

Fig. 7 provides the effluent concentration of the species at G value 11(1/s) when the flocculators spin in a counterclock-wise direction. The volume of the third basin continues to increase, the concentration at the peak point is lower, and the effluent time is delayed. However, once the concentration at the peak point is higher, the effluent time is more rapid than the flow when the flocculators spin directs clockwise. This implies that the counterclock-wise flow is a closer plug flow and is more uniform than the clockwise flow.

Fig. 8 provides the flux of the outlet at the upper part, middle part and bottom part when the flocculator spins in the clockwise direction in the case of G value 11(1/s). The upper part, middle part and bottom part are three; it divides equally at the outlet baffle in the vertical direction. The difference of the flux percentages of the three sections is reduced according to the expansion length of the

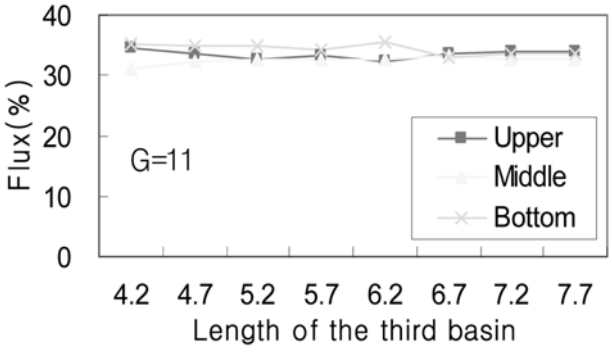

Fig. 7. The effluent concentration of species at G value 11(1/s) with counterclock-wise.

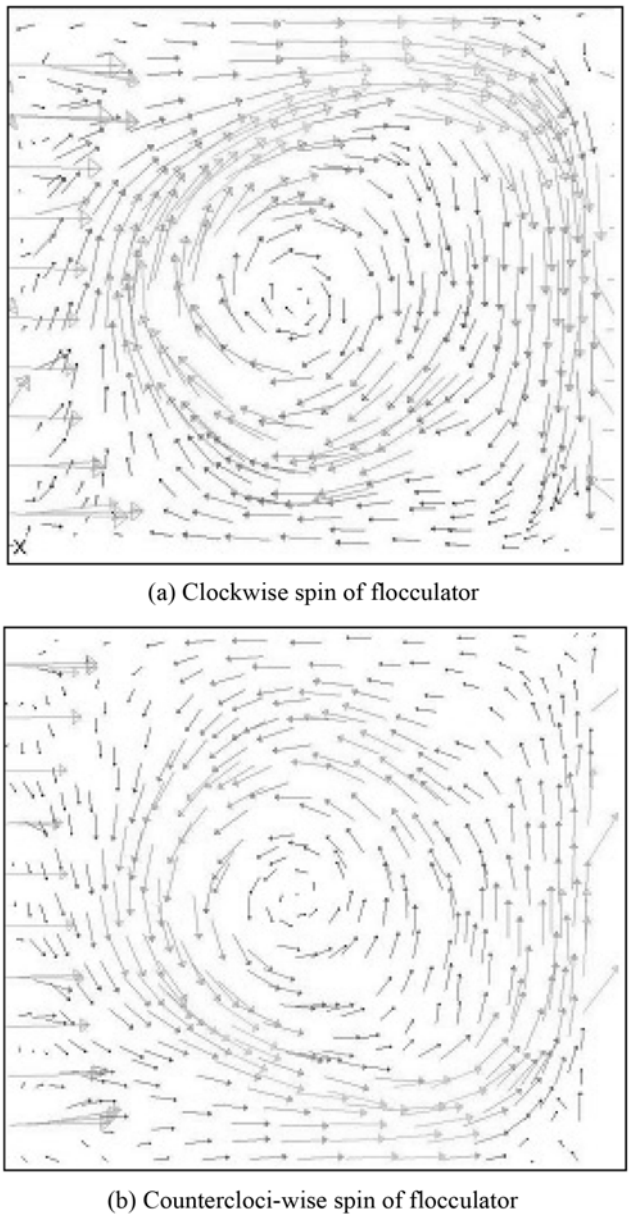

Fig. 9. The velocity vector at the third basin according to the flocculator spin.

third basin from 4.2 to 7.7. A similar result can be seen in Fig. 5, when flocculators spin clockwise in each G value. Thus, we can see that the difference of the flux percentage between the 3 sections continues to decrease according to the increase in the volume of the third basin, regardless of the spinning direction of the flocculator.

Fig. 9 indicates the vector in G value 11(1/s) according to the clockwise and counter clockwise spins of the flocculator. When the flocculator spins in the clockwise direction, the vector of the upper part is the strongest. Because the direction of flow due to the clockwise spin of the flocculator is the same about the direction of main flow, the flow of the upper part is the strongest and its flow disperses to the bottom part. On the other hand, when the flocculator is spinning in the clockwise direction, the flow of the bottom part is in the opposite direction to the main flow. The flow of the flocculator spin and the main flow run into each other. Therefore, most of the flow moves towards the outlet because the bottom of the flocculation basin is a wall. Thus, the vector and flux at the outlet are strong at the upper and bottom parts.

The counter clockwise spin of the flocculator, the direction of the flocculator spin, is the same as the main flow at the bottom part and different to the main flow at the upper part. The bottom flow is therefore the strongest and its flow disperses to the upper part. However, the vector of the upper part is not stronger than the bottom flux, because the upper part is the surface of the water rather than a wall. Therefore, the flux and vector at the upper and bottom parts are stronger than those of the middle part, regardless of the direction of spin of the flocculator.

Fig. 10 provides the standard deviation of velocity at the 3 sections of the outlet according to the length of the last third of the flocculation basin. If the standard deviation of velocity is large, the effluent flow is non-uniform and unstable. The effluent flow therefore affects the sedimentation of the bed. The standard deviation of velocity continually decreases when the volume of the last third of the flocculation basin increases and the G value is decreased. We determined the size of the buffer zone in the last third of the flocculation basin with the standard deviation of velocity at the outlet.

Fig. 11 provides the needed buffer zone compared with the third basin according to the G value at the standard deviation of velocity. For G value 10, the buffer zone needs to be about 10% compared with the last third volume for the standard deviation of velocity to be a maximum of 5. But the buffer zone needs to be about 40% of

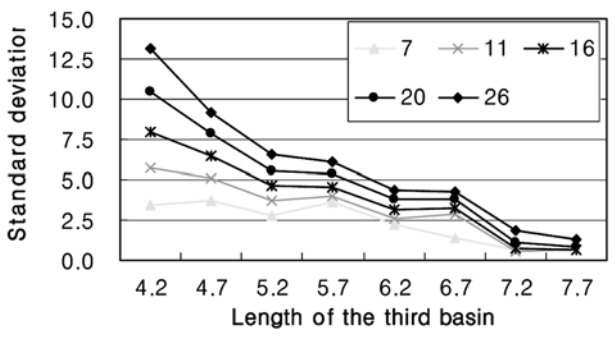

Fig. 10. Standard deviation of Velocity according to the length of the third basin.

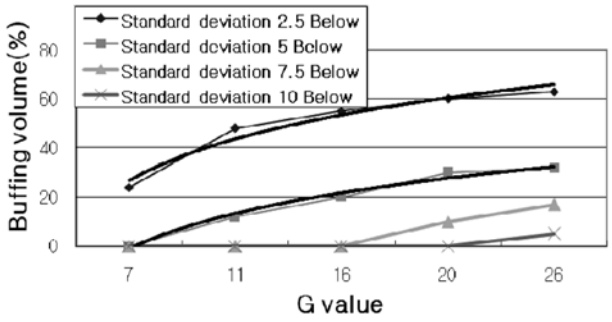

Fig. 11. Needed buffer zone compared with the third basin according to the G value.

the last third volume for the velocity of standard deviation to be half of 5. Also, for G value 16, the buffer zone needs to be about 20% and 55% for the standard deviation of velocity to be a maximum of 2.5 and 5, respectively. But for the standard deviation of velocity to be a maximum of 7.5, the buffer zone is not needed in the third basin.

As aforementioned, however, the mixing level and the generation of short circuiting flow are augmented with the increment of G value and expansion of the third basin. We therefore need to achieve a proper uniformity at a minimum of the buffer zone. If after due consideration we can determine the buffer zone, we can therefore achieve a practical application of the third party wall as an outlet wall. In addition, we can reduce the design volume of the flocculation basin and increase the efficiency of the sedimentation.

CONCLUSIONS

A simulation using CFD software was conducted in order to determine the size of the buffer zone in the last third flocculation process. Conclusions are made as follows:

The mixing level and the generation of the short circuiting flow are augmented with the increment of the G value and expansion of the third basin, and the flow in the flocculation process is therefore deteriorated.

The difference of effluent percentage of flux between the upper, middle and bottom part sections reduces according to the expansion of the third basin volume at each G value. So the effluent percentage at the three sections is more affected by the volume increase than by the G value.

The flux and vector at the upper and bottom parts are stronger than those at the middle part, regardless of whether the flocculator is spinning in a clock-wise or counter clock-wise direction.

For G value ranging from 11 to 16, the buffer zone needs to be about from 45% to 55% for the standard deviation of velocity to be a maximum of 2.5 and the buffer zone needs to be about from 10% to 20% for the standard deviation of velocity to be a maximum of 5. But for the standard deviation of velocity to be a maximum of 7.5, the buffer zone is not need in the third basin.

REFERENCES

1. S. Kawamura, John Wiley and Sons, 2nd edition, **104** (2000).
2. Y.-J. Jung and K.-S. Min, *J. Korean Society on Water Quality*, **21**,

230 (2005).
3. Prabhata, K. Swamee and A. Tyagi, *ASCE, J. Env. Eng.*, **122**, 71 (1996).
4. J. Kim and G. Y. Han, *Korean J. Chem. Eng.*, **24**, 445 (2007).
5. A. Cockx, Z. Do-quang, A. Line and M. Roustan, *Chem. Eng. Sci*., **54**, 5085 (1999).
6. R. Dupont and C. Dahl, *Water Sci. Technol*., **31**, 215 (1995).
7. P. Larwen, Report No. 1001, Department of Water Research Engineering, Lund Institute of Technology, University of Lund, Sweden (1997).
8. G. A. Ekama, J. L. Barnard, P. Krebs and J. A. McCorquofale, *JAWQ*, **173** (1997).
9. P. Krebs, *Water Sci. Technol*., **31**, 181 (1995).
10. Copyright by Fluent Inc, *Fluent6.3 user's guide*, **3**, 14.1 (2006).
11. J. Bridgeman, B. Jefferson and S. A. Parsons, Advances in Engineering Software, In Press, Corrected Proof, Available online 21 (2009).